Ecological Informatics 82 (2024) 102717

Contents lists available at ScienceDirect

Ecological Informatics

journal homepage: www.elsevier.com/locate/ecolinf

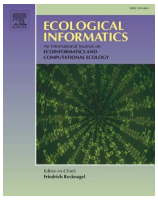

Evaluation of the monitoring capability of various vegetation indices and mainstream satellite band settings for grassland drought

Xiufang Zhu [a,b,c], Qingfen Li [a,*], Chunhua Guo [a,c]

[a] State Key Laboratory of Remote Sensing Science, Faculty of Geographical Science, Beijing Normal University, Beijing 100875, China
[b] Key Laboratory of Environmental Change and Natural Disaster, Ministry of Education, Beijing Normal University, Beijing 100875, China
[c] Beijing Engineering Research Center for Global Land Remote Sensing Products, Faculty of Geographical Science, Beijing Normal University, Beijing 100875, China

ARTICLE INFO

Keywords:
Drought monitoring
Canopy spectrum
Grassland
Vegetation index

ABSTRACT

In the context of global climate change and increasing human activities, grassland drought has become increasingly severe and complex. The monitoring of grassland drought is crucial for reducing drought-related losses and ensuring national ecological security. This study used the coupled PROSPECT and SAIL radiative transfer models (PROSAIL) to simulate canopy reflectance, considering factors such as grassland growth stages and varying drought conditions. Our objective was to reveal the spectral response characteristics of grasslands to varying drought conditions and identify sensitive spectral bands suitable for drought monitoring during different grassland growth stages. We aligned commonly available satellite bands from moderate resolution imaging spectroradiometer (MODIS), Sentinel 2, Landsat 8, WorldView 2, and Gaofen 2 (GF 2) with these sensitive bands to assess the capabilities of existing satellite data for drought monitoring. Furthermore, this research evaluated the suitability of 16 commonly used remote sensing vegetation indices for grassland drought monitoring, including Normalized Difference Vegetation Index (NDVI), Enhanced Vegetation Index (EVI), Ratio Vegetation Index (RVI), Difference Vegetation Index (DVI), Modified Soil Adjusted Vegetation Index (MSAVI), Atmospherically Resistant Vegetation Index (ARVI), Modified Normalized Difference Water Index (MNDWI), Global Vegetation Moisture Index (GVMI), Land Surface Water Index (LSWI), Visible and Shortwave Infrared Drought Index (VSDI), Water index(WI), Moisture Stress Index(MSI), Normalized Difference Water Index(NDWI), Normalized Difference Infrared Index (NDII), Photochemical Reflectance Index (PRI), and Optimized Soil-Adjusted Vegetation Index (OSAVI). The simulation and analysis results revealed: 1) Grassland in different growth stages exhibit similar sensitivities to certain spectral bands, namely those within the ranges of 540 nm–720 nm, 1250 nm–1690 nm, 1805 nm–2190 nm, and 2264 nm–2500 nm, which are more sensitive to various drought conditions. 2) Suitable vegetation indices for both growing and stable stages include NDII, MSI, PRI, LSWI, and GVMI, with silhouette coefficients exceeding 0.6 for the growing stage and 0.7 for the stable stage. The least suitable vegetation index is DVI, with an average silhouette coefficient of 0.15 over the entire growth stage. 3) From the spectral band perspective, among the five assessed satellites, MODIS Band 7 exhibits the highest sensitivity to water content across all satellite bands. MODIS's band configuration is most suitable for monitoring grassland drought during different growth stages, while WorldView 2's band configuration is the least suitable.

1. Introduction

Grasslands, as one of the most widely distributed vegetation types in the world, represent a significant ecosystem type with crucial ecological importance in terms of windbreaks, sand fixation, regional ecological balance maintenance, and climate regulation (Li et al., 2021a). Compared to other ecosystems, grasslands are more susceptible to drought (Ding et al., 2020; Henchiri et al., 2020; Peng et al., 2012). Drought in grasslands not only directly impacts livestock and agriculture but also triggers a range of ecological issues, such as grassland degradation and dust storms (Liu et al., 2022). The increasing frequency and severity of droughts due to global warming further exacerbate this situation (Mpelasoka et al., 2008). Additionally, the impacts of drought on grassland ecosystems become more complex when coupled with human activities (Zhang et al., 2018). Therefore, improving the monitoring and early warning systems for grassland drought is crucial for effectively

* Corresponding author at: No. 19, Xinjiekouwai St, Haidian District, Beijing 100875, China.
E-mail address: 202321051201@mail.bnu.edu.cn (Q. Li).

https://doi.org/10.1016/j.ecoinf.2024.102717
Received 1 February 2024; Received in revised form 30 June 2024; Accepted 4 July 2024
Available online 6 July 2024

mitigating its effects and minimizing associated losses. This is of paramount importance for achieving national ecological security.

Remote sensing data, characterized by multitemporal, multispectral, and multiangle attributes, facilitates the acquisition of extensive, long-term surface information series such as soil, vegetation, and temperature (Duarte et al., 2014; Li et al., 2021b; Li et al., 2023). This data enables both qualitative and quantitative analyses of soil water deficits and vegetation water stress from diverse perspectives, proving invaluable in drought monitoring applications. According to previous statistics, the moderate resolution imaging spectroradiometer (MODIS), Landsat, Sentinel, Gaofen (GF), and WorldView are currently the five most influential satellites in various remote sensing related research (Zhao et al., 2022). Among freely available datasets, Landsat and MODIS stand out for their extensive temporal coverage, making them particularly suitable for long-term drought monitoring (Gessner et al., 2023; Sall et al., 2021), while Sentinel data, characterized by its higher temporal, spatial, and spectral resolutions, has been also extensively utilized in drought monitoring across various ecosystems such as forests and agricultural fields (Varghese et al., 2021; West et al., 2019). For example, Zhao et al. (2023) assessed the capability of MODIS-derived Normalized Difference Vegetation Index (NDVI), Enhanced Vegetation Index (EVI), and Gross Primary Productivity (GPP) products respond to different levels of drought severity in Inner Mongolia grasslands from 2002 to 2020. Yu and Guo (2023) proposed a revised vegetation health index (VHI) to monitor drought severity of mixed grasslands in the Grasslands National Park of Canada using historical Landsat imagery. Kowalski et al. (2022) quantified drought effects in a Central European grassland region from 2017 to 2020 based on the Sentinel-2 time series data.

Drought monitoring based on remote sensing often relies on various remote sensing indices (Alahacoon and Edirisinghe, 2022; Liu et al., 2020). For instance, indices reflecting water stress in vegetation leaves or canopy temperature, such as the Moisture Stress Index (MSI) (Hunt Jr et al., 1987), the Water Index (WI) (Peñuelas et al., 1997), the Normalized Difference Water Index (NDWI) (Gao, 1996), the Global Vegetation Moisture Index (GVMI) (Ceccato et al., 2002), the Normalized Difference Vegetation Index (NDVI) (Tucker, 1979), the Vegetation Condition Index (VCI) (Kogan, 1990), the Ratio Vegetation Index (RVI) (Zhou et al., 2021), and the Atmospherically Resistant Vegetation Index (ARVI) (Perry and Roberts, 2008) are commonly employed. Therefore, the development of new remote sensing indices (Chang et al., 2021) and the performance evaluation of existing remote sensing indices in drought monitoring (Behifar et al., 2023; Liu et al., 2020; Wei et al., 2021) have become two key directions in remote sensing index research on drought monitoring. The essence of developing remote sensing indices is to identify sensitive spectral bands affected by drought and then derive remote sensing indices through combinations of these sensitive bands (Zhang et al., 2013). Evaluating the capabilities of existing remote sensing indices in drought monitoring often relies on remote sensing datasets. Various remote sensing indices are calculated as extensively as possible, followed by the analysis of the correlation between these indices and other existing indicators of drought, such as meteorological drought indices and soil moisture (Chang et al., 2017; Ghasempour et al., 2024). Hyperspectral data, characterized by their high spectral resolution, strong spectral continuity, and rich spectral information, is the preferred data type for both research directions.

Hyperspectral dataset acquisition under drought stress conditions can be broadly categorized into two methodologies: field control experiments and model simulations. Field control experiments involved the establishment of reference and drought stress groups within experimental fields, with varying vegetation drought stress conditions achieved through controlled irrigation and rain-shielding equipment. Hyperspectral data, along with corresponding physiological and biochemical indicators (such as leaf area index and chlorophyll content) and environmental indicators (like temperature and soil moisture), are then measured under these diverse drought stress conditions. For instance, Zhang and Zhou (2015) measured canopy water content (CWC) of maize in the north plain China with varying irrigation levels to assess the capability of different vegetation indices in estimating CWC. Li et al. (2022) exposed wheat to drought stress at different growth stages in the greenhouse in Beijing, China, analyzing the spectral curve characteristics of the wheat canopy under different drought stress conditions. However, field experiments are often hindered by their lengthy durations, significant financial investment, substantial labor costs, and limited data collection capacity, making it difficult to gather a large volume of empirical data across different growth stages and drought stress conditions. Model simulation, on the other hand, simulates vegetation spectral curves under drought stress conditions based on radiative transfer models. The PROSPECT leaf optical properties model and SAIL canopy bidirectional reflectance model are widely used in related studies. By coupling the PROSPECT and SAIL models, the PROSAIL model can quantitatively describe the influence of characteristics such as pigment content, moisture, leaf area index (LAI), and other parameters on reflectance spectra. This allows for forward simulation of canopy spectra and backward inversion of physiological parameters (English et al., 2020). Using the PROSAIL model allows for the analysis of spectral bands that are more sensitive to changes in different physiological parameters. This is advantageous for investigating the response characteristics of vegetation physiological parameters under varying moisture conditions, as well as for conducting a mechanistic analysis of sensitive spectral bands and monitoring indices (Berger et al., 2018). Zhang et al. (2017) conducted irrigation control experiments on winter wheat. Through a global sensitivity analysis using the PROSAIL model, they found that leaf reflectance is more sensitive to changes in leaf water content compared to canopy reflectance. Based on the PROSAIL model and measured spectral data, their experiment revealed that using NDWI is effective in estimating both leaf and CWC. Xing et al. (2021) utilized the PROSAIL model to simulate canopy spectra at different growth stages of winter wheat, establishing models that correlate various spectral indices with LAI and chlorophyll content (CCD). Their findings suggest indices derived from spectral and physiological characteristics could better estimate LAI and CCD during different growth stages of winter wheat. Compared to field experiments, simulation methods based on the PROSAIL model are cost-effective and user-friendly, and can provide a large number of simulated spectral data under various conditions, facilitating subsequent quantitative analyses.

Current research efforts, whether aimed at the development of novel drought indices or the evaluation of existing ones, have predominantly focused on drought monitoring of crops, such as wheat and maize (Li et al., 2021c; Li et al., 2022; Lijuan et al., 2017). Research on drought monitoring in grasslands is relatively limited, mostly using meteorological drought indices, soil moisture indices, and composite drought indices (Behifar et al., 2023). Current research has demonstrated that vegetation indices effectively characterize the health status of vegetation under stress conditions by reflecting changes in vegetation water content and greenness (Ashraf et al., 2022; Cârlan et al., 2020; Jin and Wang, 2016). However, there is limited comprehensive assessments regarding the capacity of vegetation indices to monitor grassland drought (Almeida-Ñauñay et al., 2022; Chang et al., 2021; Li et al., 2021d; Liu et al., 2021). Additionally, although the PROSAIL model has been proven to be suitable for simulating grassland spectra (Atzberger et al., 2013; Féret et al., 2017), there are few studies on simulating grassland spectra under drought stress conditions. Therefore, exploring the spectral response characteristics of grasslands at different growth stages to varying drought conditions and evaluating the applicability and capability of existing vegetation indices in grassland drought monitoring is significant for enhancing the accuracy and precision of grassland remote sensing drought monitoring.

Taking all of the above into consideration, this study uses the PROSAIL model in conjunction with empirically measured physiological parameters of grassland and soil reflectance data under diverse humidity levels to simulate spectral curves of grassland at different soil moisture

conditions and growth stages. On this basis, the study aims to answer three key questions: 1) What spectral band ranges exhibit the highest sensitivity of grassland canopy reflectance to drought? 2) From a spectral perspective, which of the five mainstream satellites (GF-2, Landsat-8, Sentinel-2, WorldView-2, and MODIS) is the most suitable for drought monitoring? 3) How do the 16 commonly used vegetation indices perform in drought monitoring? The innovation of this study mainly lies in comprehensively evaluating the ability of 16 commonly used remote sensing indicators and 5 commonly used satellites to monitor grassland drought with consideration of grass growth stage and drought intensity for the first time. The answers to these questions will serve as a reference for the selection of data and indicators in drought monitoring and provide theoretical support for the design of novel sensors and remote sensing drought indices.

2. Methods

2.1. Simulating grassland spectra under various drought conditions using PROSAIL

The PROSAIL model is developed by coupling the PROSPECT model with the SAIL model (Jacquemoud and Baret, 1990). PROSPECT model is first used to simulate leaf reflectance (ρ_l) and transmittance (τ_l) in the range of 400 to 2500 nm, and then ρ_l and τ_l derived from the PROSPECT model combined with other parameters are input to the SAIL model to simulate canopy bidirectional reflectance (Jupp and Strahler, 1991). In this study, PROSPECT-D model (Eq. (1)) is employed, in which the parameters include leaf structural parameter (N), leaf chlorophyll content (C_{ab}), leaf equivalent water thickness (C_w), dry matter content (C_m), brown pigment content (C_{brown}) and carotenoid (C_{CX}) (Féret et al., 2017). Except for ρ_l and τ_l derived from the PROSPECT model, the SAIL model (Eq. (2)) requires canopy structural parameters, such as LAI and leaf inclination distribution (LIDF), viewing geometry parameters, such as sun zenith angle (*tts*), viewing zenith angle (*tto*), relative azimuth angle between sun and sensor (*psi*), hotspot effect (*hot*), and soil reflectance (ρ_s) (Verhoef, 1984).

$$(\rho_l, \tau_l) = \mathrm{PROSPECT}(N, C_{ab}, C_w, C_{CX}, C_m, C_{brown}) \tag{1}$$

$$\rho = \mathrm{SAIL}(\mathrm{LAI}, \mathrm{LIDF}, \rho_l, \tau_l, \rho_s, hot, tts, tto, psi) \tag{2}$$

In order to observe the response of grassland reflectance to drought at different production stages, referring to the physiological parameters of grasslands under different growth stages and drought conditions measured by Bayat et al. (2016), this study defined two different grassland growth stages (growing stage and stable stage), and set specific PROSAIL model parameters for each stage. The growing stage was characterized by rapid changes in LAI, which increases from 2.3 to 3 under no water stress conditions; during the stable stage, LAI remained basically unchanged and remained around 3 under no water stress conditions. For each growth stage, we further defined three scenarios: no drought, mild drought, and severe drought. Mild drought was defined as the stage from cessation of watering to visible signs of stress on the grassland, characterized by curling and shrinking of leaves, dull luster, etc., with a decrease in Cab and Cw. Severe drought was defined as the stage in which water stress continues to worsen after the occurrence of mild drought, characterized by yellowing, wilting, and falling of leaves, with a continuous decrease in all parameters except for C_{brown}. In addition, considering the different soil moisture corresponding to different drought conditions, referring to the definition of agricultural drought (West et al., 2019) and the soil moisture data measured by Bayat et al. (2016) under different drought conditions, different soil reflectance curves under varying soil moisture conditions were input PROSAIL model to simulate canopy spectral curves of grassland under different drought conditions. Specifically, in the study of Bayat et al. (2016), the soil moisture of saturated soil was approximately between $0.3 m^3 \bullet m^{-3}$ and $0.4\ m^3 \bullet m^{-3}$. Therefore, we set the soil reflectance when the soil moisture decreases by about 50% ($0.17 m^3 \bullet m^{-3}$) as the soil reflectance under mild drought conditions, and the reflectance of dry soil (soil moisture content of $0.02\ m^3 \bullet m^{-3}$) as the soil reflectance under severe drought conditions. Table 1 summarizes the distribution and ranges of parameters used in the PROSAIL model in this study.

2.2. Analyzing bands sensitive to changes in grassland moisture content

Analysis of variance (ANOVA) is a statistical method employed to ascertain whether a specific variable significantly influences the observed variable. This is achieved by examining the variance of the observed variable while simultaneously controlling for other variables. In this study, one-way ANOVA is used to determine if there are significant differences in the simulation results for the same wavelength under different drought conditions. The Eqs. (3)–(5) for calculating it is as follows:

(1) Calculate the between-group variance S_A:

$$S_A = \sum_{i=1}^{s} \left[(\overline{x_i} - \overline{x})^2 n_i \right] \tag{3}$$

(2) Calculate the within-group variance S_E:

$$S_E = \sum_{i=1}^{s} \sum_{j=1}^{n_i} \left(x_{ij} - \overline{x_i} \right)^2 \tag{4}$$

(3) Calculate the F ratio

$$F = \frac{S_A/(s-1)}{S_E/(n-s)} \tag{5}$$

In the equations provided:

- $\overline{x_i}$ is the sample mean for the ith treatment.
- $\overline{x_{ij}}$ is the j^{th} observation f on the i^{th} treatment.
- $\overline{x}$ is the grand mean of the observations.

The calculated F ratios are compared to the expected values from the F distribution. If the computed F ratio significantly exceeds the expected value (assuming a sufficiently small p value), the null hypothesis will be rejected, indicating that there are significant differences among the groups.

In this study, a variance analysis is conducted to examine the reflectance values at each wavelength under different drought conditions. The derived F ratios are used to assess the sensitivity of each wavelength between 400 nm and 2500 nm to changes in moisture content. A higher F ratio indicates a greater difference in reflectance values under different drought conditions, indicating that the wavelength is more sensitive to changes in moisture content and is suitable for monitoring grassland drought. The study computes two sets of F ratios: one set involves the one-way ANOVA of data under normal and severe drought conditions, and the other set involves a one-way ANOVA of data under no drought, mild drought, and severe drought conditions, treating them as three separate groups. To better extract bands sensitive to moisture changes based on the F ratio curve, the study calculates the first derivative of the F ratio curve. Points where the first derivative is zero represent inflection points in the curve's trend. By identifying these points ($f'(x) = 0$), bands with higher F ratios can effectively be extracted, indicating the bands sensitive to moisture changes.

2.3. Assessing the capability of various vegetation indices for monitoring grassland drought

This study selected 16 commonly used vegetation indices to assess

Table 1
Specific ranges for input parameters used for PROSAIL model.

	Parameter	Description	Unit	Growth Stage	Range	Distribution
Leaf	N	Leaf structural parameter		Undifferen-tiated	1.5	Fixed
	C_{ab}	Leaf chlorophyll content	ug/cm^2	Growing stage	No drought: 21.35–22.49 Mild drought: 18.44–21.12 Severe drought: 10.53–18.44	Gaussian
				Stable stage	No drought: 21.52–22.89 Mild drought: 7.02–10.53 Severe drought:3.60–7.02	
	C_{cx}	Carotenoid	ug/cm^2	Undifferenti-ated	5	Fixed
	C_{brown}	Brown pigment content		Growing stage	No drought: 0.023–0.037 Mild drought: 0.028–0.032 Severe drought:0.032–0.101	Gaussian
				Stable stage	No drought: 0.012–0.024 Mild drought: 0.101–0.160 Severe drought:0.160–0.297	
	C_w	Leaf equivalent water thickness	cm	Growing stage	No drought: 0.0059–0.0062 Mild drought: 0.0036–0.0057 Severe drought:0.0019–0.0036	Gaussian
				Stable stage	No drought: 0.0062–0.0073 Mild drought: 0.0011–0.0019 Severe drought:0.0010–0.0011	
	C_m	Dry matter content	g/cm^2	Growing stage	No drought: 0.00161–0.00221 Mild drought: 0.00166–0.00170 Severe drought: 0.00170–0.00174	Gaussian
				Stable stage	No drought: 0.00221–0.00251 Mild drought: 0.00162–0.00177 Severe drought:0.00151–0.00162	
	LAI	Leaf area index		Growing stage	No drought: 2.31–3.02 Mild drought: 2.34–2.53 Severe drought:2.53–2.66	Gaussian
				Stable stage	No drought: 2.96–3.10 Mild drought: 2.31–2.57 Severe drought:1.61–2.31	
	LIDFa	Leaf angle distribution	°		−0.35	Fixed
	LIDFb		°	Undifferentia-ted	−0.15	Fixed
	hspot	Hot spot size parameter			0.05	Fixed
Soil	psoil	Soil brightness factor		Undifferentia-ted	1	Uniform
Other	tts	Sun zenith angle	°		0–60	Uniform
	tto	View zenith angle	°	Undifferentia-ted	0–60	Uniform
	psi	Relative azimuth angle	°		0–360	Fixed
	skyl	Fraction of diffuse			Calculated from model	

their suitability for monitoring grassland drought (as shown in Table 2). In the equations, the variables BLUE, GREEN, RED, NIR, and SWIR denote the respective spectral bands of satellite sensors, encompassing the blue, green, red, near-infrared, and shortwave infrared bands. When calculating vegetation indices using satellite bands, the initial step involves the weighted summation of simulated reflectance values at different wavelengths within the designated sensor-specific band ranges, in accordance with the sensor's spectral response function. Subsequently, this summation is transformed into the broadband reflectance of the sensor, followed by the computation of commonly used vegetation indices.

In this study, silhouette coefficient method (Bagirov et al., 2023) and the separation index (Kaufman and Remer, 1994) were used to evaluate the ability of vegetation indices to distinguish different drought intensities. The silhouette coefficient method comprehensively considers the degree of intra class clustering (i.e. the degree of clustering of vegetation index values under the same drought condition) and the degree of inter class separation (i.e. the degree of separation of vegetation index values under different drought conditions) to reflect the clustering effect. The silhouette coefficient S is defined as shown in Eq. (6).

$$S(i) = \frac{d_{rest}(i) - d_s(i)}{max[d_{rest}(i), d_s(i)]} \tag{6}$$

where $S(i)$ represents the silhouette coefficient, with values ranging from −1 to 1. A higher $S(i)$ indicates a more reasonable classification of samples and better clustering under the chosen classification method. Conversely, a lower $S(i)$ closer to −1 suggests a less reasonable classification and poorer sample clustering, indicating reduced discriminative capacity in delineating the distribution ranges of vegetation indices under different drought conditions.

The separation index (SI) is used to evaluate the separation ability of two classes, which is defined as shown in Eq. (7).

$$SI = \frac{|u_1 - u_2|}{\sigma_1 + \sigma_2} \tag{7}$$

where u and σ are the mean value and standard deviation value of same vegetation index under different drought conditions. Higher SI values show better separation between two classes.

2.4. Assessment of the potential of different satellite data for monitoring grassland drought

This study examines the potential of satellite data for monitoring grassland drought from two perspectives. First, by calculating the mean values based on the F ratios within the wavelength ranges specified by satellite sensors, the canopy spectra of different bands from different satellite sensors in response to moisture conditions during different growth stages of grassland are compared. This analysis aims to identify the satellites and their respective spectral bands that exhibit the highest sensitivity to drought stress. Second, this study evaluates the capability of satellites for grassland drought monitoring by assessing the silhouette coefficients and SI of 10 vegetation indices computed from simulated satellite band reflectance data (as shown in Table 2).

Table 2
The vegetation indices considered for evaluation.

Group	Index	Formulas	Satellites
Calculated from specific wavelengths	Normalized Difference Infrared Index (NDII) (Jackson et al., 2004)	$\frac{R_{850}-R_{1650}}{R_{850}+R_{1650}}$	None
	Moisture Stress Index (MSI) (Hunt Jr et al., 1987)	$\frac{R_{1600}}{R_{820}}$	
	Normalized Difference Water Index (NDWI) (Gao, 1996)	$\frac{R_{860}-R_{1240}}{R_{860}+R_{1240}}$	
	Photochemical Reflectance Index (PRI) (Gamon et al., 1992)	$\frac{R_{531}-R_{570}}{R_{531}+R_{570}}$	
	Water index (WI) (Peñuelas et al., 1997)	$\frac{R_{900}}{R_{970}}$	
Calculated from NIR and visual bands	Optimized Soil-Adjusted Vegetation Index (OSAVI) (Rondeaux et al., 1996)	$(1+0.16)\times\frac{(R_{800}-R_{670})}{(R_{800}+R_{670}+0.16)}$	MODIS; Sentinel 2; Landsat 8; Worldview 2; GF 2
	Atmospherically Resistant Vegetation Index (ARVI) (Kaufman and Tanre, 1992)	$\frac{NIR-2RED+BLUE}{NIR+2RED+BLUE}$	
	Difference Vegetation Index (DVI) (Demetriades-Shah et al., 1990)	$NIR-RED$	
	Enhanced Vegetation Index (EVI) (Huete et al., 2002)	$\frac{NIR-RED}{NIR+6RED-7BLUE+1}$	
	Modified Soil Adjusted Vegetation Index (MSAVI) (Qi et al., 1994)	$0.5(2\mathrm{NIR}+1-\sqrt[2]{2(2NIR+1)-8(NIR-RED)}$	
	Normalized Difference Vegetation Index (NDVI) (Tucker, 1979)	$\frac{NIR-RED}{NIR+RED}$	
	Ratio Vegetation Index (RVI) (Jordan, 1969)	$\frac{NIR}{RED}$	
Calculated from SWIR and other bands	Global Vegetation Moisture Index (GVMI) (Ceccato et al., 2002)	$\frac{(NIR+0.1)-(SWIR+0.02)}{(NIR+0.1)+(SWIR+0.02)}$	MODIS; Sentinel 2; Landsat 8
	Land Surface Water Index (LSWI) (Xiang et al., 2020)	$\frac{NIR-SWIR}{NIR+SWIR}$	
	Modified Normalized Difference Water Index (MNDWI) (Szabo et al., 2016)	$\frac{GREEN-SWIR}{GREEN+SWIR}$	
	Visible and Shortwave Infrared Drought Index (VSDI) (Zhang et al., 2013)	$1-[(\mathrm{SWIR}-\mathrm{BLUE})+(\mathrm{RED}-\mathrm{BLUE})]$	

3. Results

3.1. Simulation spectra of grassland

In this study, the PROSAIL model was used to simulate the spectral reflectance of grassland canopies during different growth stages and varying drought conditions, resulting in a total of 8640 simulated spectral curves. The average reflectance under different conditions is shown in Fig. 1. Overall, the variation characteristics of canopy reflectance in the two growth stages under different drought conditions are similar. Except for the wavelength range of 720 nm to 1200 nm during the stable growth stage, in which the reflectance decreases as drought severity increases, the canopy reflectance increases with increasing drought severity in both growing stage and stable growth stage.

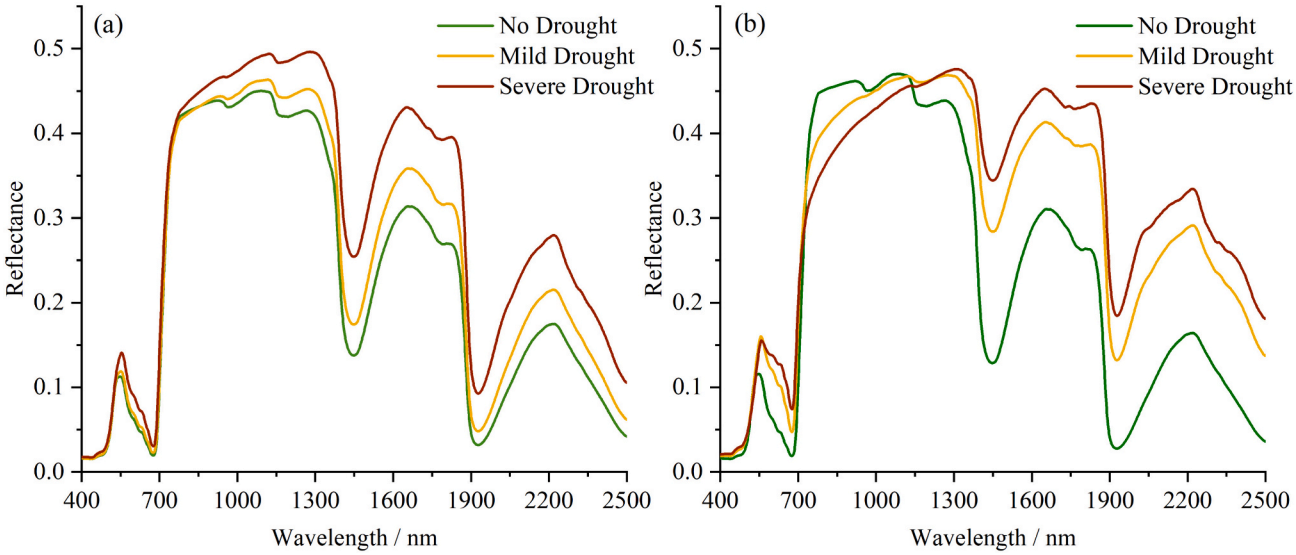

Fig. 1. Simulation of grassland canopy reflectance during the growing stage (a) and the stable stage (b).

3.2. The spectral bands sensitive to changes in grassland moisture content

Four distinct bands sensitive to changes in moisture content were extracted during the growing and stable stages of grassland, as shown in Fig. 2. Fig. 2a displays the results of two sets of F ratios obtained during the growing stage, while Fig. 2b presents the first-order derivative of the F ratios during this stage. Similarly, Fig. 2c shows the results of two sets of F ratios obtained during the stable stage, and Fig. 2d presents the first-order derivative of the F ratios during the stable stage. It is evident that bands with relatively high F ratios primarily occur in the visible and shortwave infrared spectral ranges. The bands sensitive to moisture content in the visible spectrum are between approximately 540 nm and 720 nm. Compared to the shortwave infrared range, the F ratios in this interval are relatively lower but still exhibit a pronounced contrast with the surrounding wavelengths. In the shortwave infrared region, three prominent bands with high F ratios were observed, spanning from 1250 nm to 1690 nm, 1805 nm to 2190 nm, and 2264 nm to 2500 nm. These findings indicate that grassland canopy reflectance is most sensitive to changes in moisture conditions within these bands, with peak F ratios occurring at approximately 1450 nm and 1930 nm. Previous studies have indicated that these positions in grassland reflectance curves correspond to two major absorption valleys, primarily influenced by leaf cell sap, cell membranes, and water content in absorption bands (Qin et al., 2021; Ranjan et al., 2017). These results align with our fundamental understanding of vegetation reflectance characteristics.

Analyzing the F ratio curves in the same growth stage reveals that the moisture-sensitive bands do not exhibit significant differences among different drought conditions. Although the F ratios obtained from the ANOVA for the three conditions of no drought, drought, and severe drought are smaller than those obtained from the ANOVA for the two conditions of no and severe drought, all four F ratio curves show statistically significant differences in the simulated results of the four sensitive bands mentioned above across various drought conditions.

Comparing the sensitivity of bands between the two growth stages, no significant differences in moisture-sensitive bands are observed. However, during the stable stage, the F ratios in the visible spectrum are higher than those in the growing stage, with a small region of significantly higher F ratios observed between 750 nm and 1000 nm. Conversely, during the growing stage, F ratios are higher at approximately 970 nm and 1200 nm, which coincide with the leaf water absorption bands. These differences indicate the varying responses of grassland canopy moisture content under different drought conditions during the two growth stages.

3.3. Drought monitoring capability for different vegetation indices

In this study, S and SI were used to assess the drought monitoring capability of different vegetation indices. The assessment results of S and SI are consistent. In order to reduce space and information redundancy, we only present the evaluation results based on silhouette coefficient in this section. The evaluation results based on separation index can be found in Appendix.

A higher silhouette coefficient indicates a greater capacity to differentiate the distribution intervals of the same vegetation index under different drought conditions. For instance, when computing fixed-wavelength vegetation indices based on simulated spectral curves

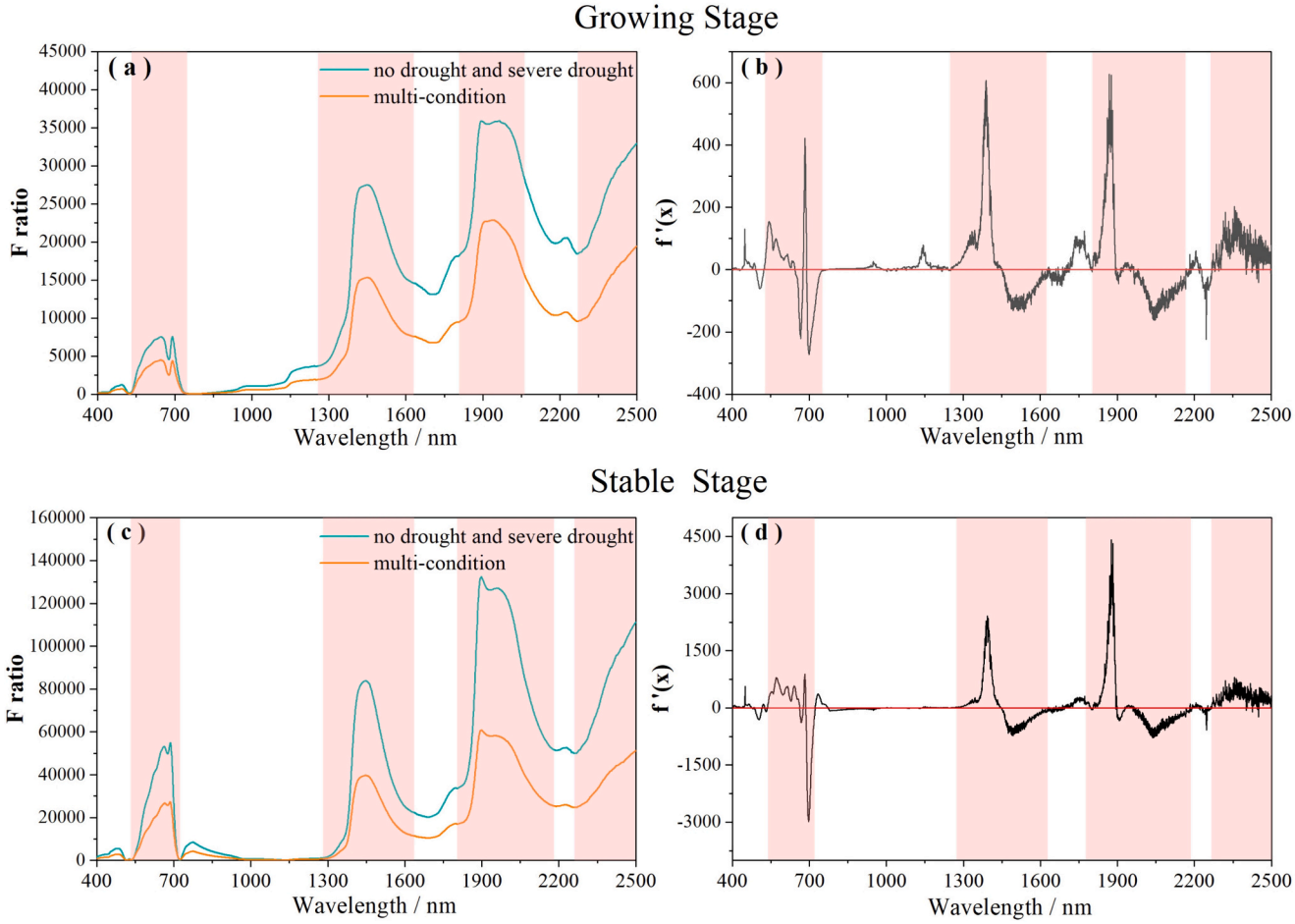

Fig. 2. Curve of F ratios for different wavelengths. (a) Curve of F ratios during the growing stage; (b) first derivative of F ratios during the growing stage; (c) Curve of F ratios during the stable stage; (d) first derivative of F ratios during the stable stage. (Note: the shaded area represents the sensitive band range).

during periods of stability (as shown in Fig. 3), it can be observed that the MSI (S = 0.797) and PRI (S = 0.793) exhibit significant differentiation in vegetation index values under various drought conditions. This suggests that these indices can effectively distinguish the level of drought in the grassland based on their index values. In contrast, the NDWI (S = 0.653) and WI (S = 0.671) show a higher degree of overlap in the distribution range of vegetation indices under different drought conditions. Consequently, when the computed results fall within this overlapping region, it becomes challenging to accurately assess the level of drought in the grassland. This evaluation result is consistent with previous studies on the relationship between vegetation indices and vegetation water content(Colombo et al., 2008; Wang et al., 2015).

The silhouette coefficient results for the 16 selected vegetation indices are presented in Fig. 4. Fig. 4a, c and e display the results for various vegetation indices during the growing stage revealing that the PRI exhibits the highest silhouette coefficient (S = 0.753), indicating it is the most suitable index for monitoring drought during this growth stage. Following PRI, GVMI, LSWI, NDII, and MSI all demonstrate silhouette coefficients greater than 0.6. Conversely, the remaining vegetation indices perform poorly, with DVI, EVI, MSAVI and OSAVI all exhibiting silhouette coefficients below 0, rendering them unsuitable for drought monitoring during the grassland growing period.

Fig. 4b, d and f present the silhouette coefficient results for the various vegetation indices during the stable stage. Compared to during the growing period, all vegetation indices exhibit higher silhouette coefficient values during the stable stage. This indicates that the differentiation of vegetation index values under different drought conditions is enhanced during the stable period. The vegetation indices with the highest silhouette coefficient values are LSWI and GVMI, both of which achieved silhouette coefficients of approximately 0.8 when calculated using data from different satellites. Subsequently, NDII, MSI, PRI and ARVI all achieved silhouette coefficients exceeding 0.7, while DVI performed the least effectively.

In summary, vegetation indices that use shortwave infrared bands in their calculation formulas perform relatively well during both the growing and stable stages. Vegetation indices using near-infrared bands in their calculation formulas perform poorly during the growing stage but relatively well during the stable stage. Indices suitable for drought monitoring in both the growing and stable stages include NDII, MSI, PRI, LSWI, and GVMI, while DVI is not suitable for either stage.

3.4. Drought monitoring potential of different satellite data sources

The bar chart in Fig. 5 presents the mean F ratios, indicating that as grassland grows, the drought monitoring capabilities of five different satellites in various spectral bands significantly improve for monitoring drought stress. When examining the drought detection capabilities across different spectral bands, it is evident that in both growth stages, the highest mean F ratios are found within the red and shortwave infrared (SWIR) bands. This suggests that within these wavelength ranges, reflectance differences are more pronounced under different drought conditions, making them more suitable for drought monitoring. Conversely, the blue and near-infrared (NIR) bands exhibit the lowest F ratios, indicating lower capabilities for drought monitoring when using these bands individually.

In the analysis of the capabilities of drought monitoring in different spectral bands for various satellites, during both growth stages, Sentinel 2 and Landsat 8 consistently exhibit higher mean F ratios within the green spectral band compared to other satellites. In the red spectral band during the growing stage, MODIS shows higher mean F ratios compared to other satellites, while during the stable stage, Sentinel 2 and Landsat 8 exhibit higher mean F ratios, indicating that MODIS has stronger drought monitoring capabilities in this band compared to other satellites. Within the NIR band, GF 2 and WorldView 2 consistently exhibit higher mean F ratios compared to other satellites during the stable stage. However, it is important to note that the sensors on these two satellites do not include a SWIR band. Comparing the drought monitoring capabilities among the remaining three satellites within the SWIR region, MODIS's third SWIR band (band 7) has the highest mean F ratios, indicating the strongest drought monitoring capability, while the first SWIR band (band 5) performs the poorest compared to the other SWIR bands. Sentinel 2 and Landsat 8 both demonstrate stable drought monitoring

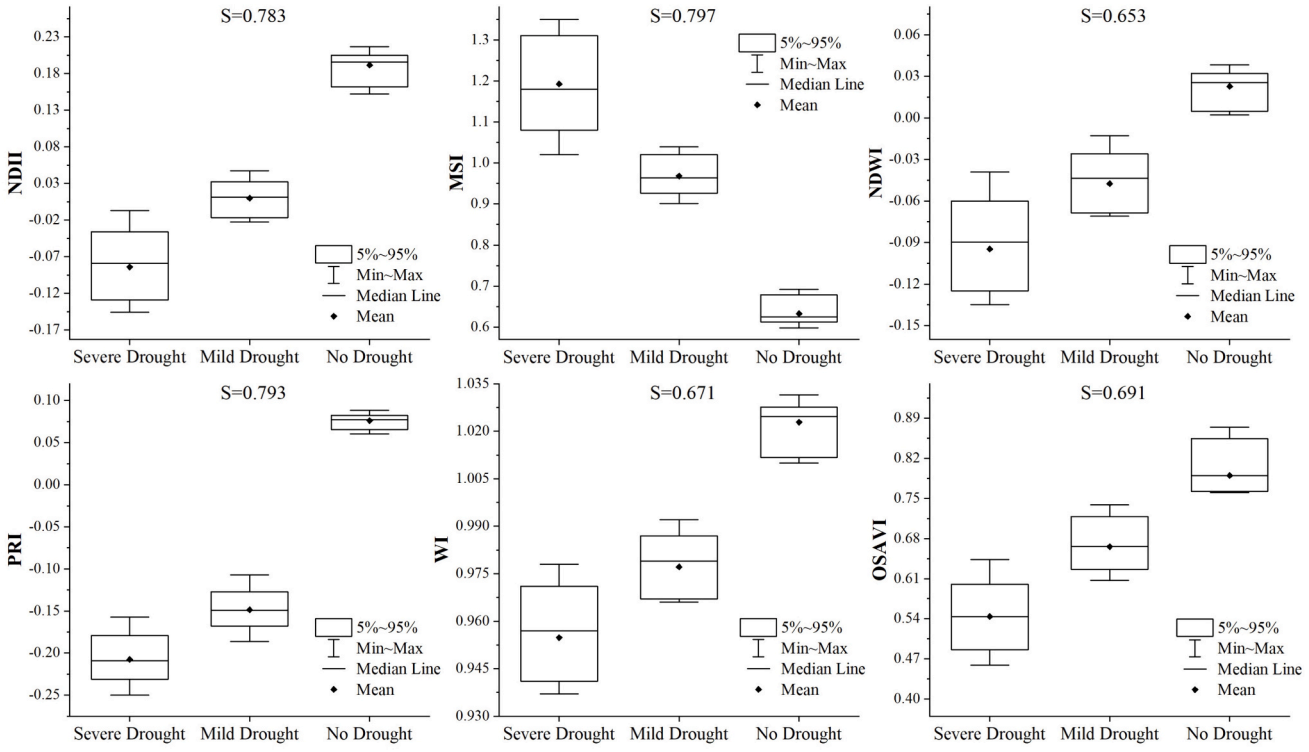

Fig. 3. Box plots of 6 vegetation indices calculated from specific wavelengths during the stable stage of grassland.

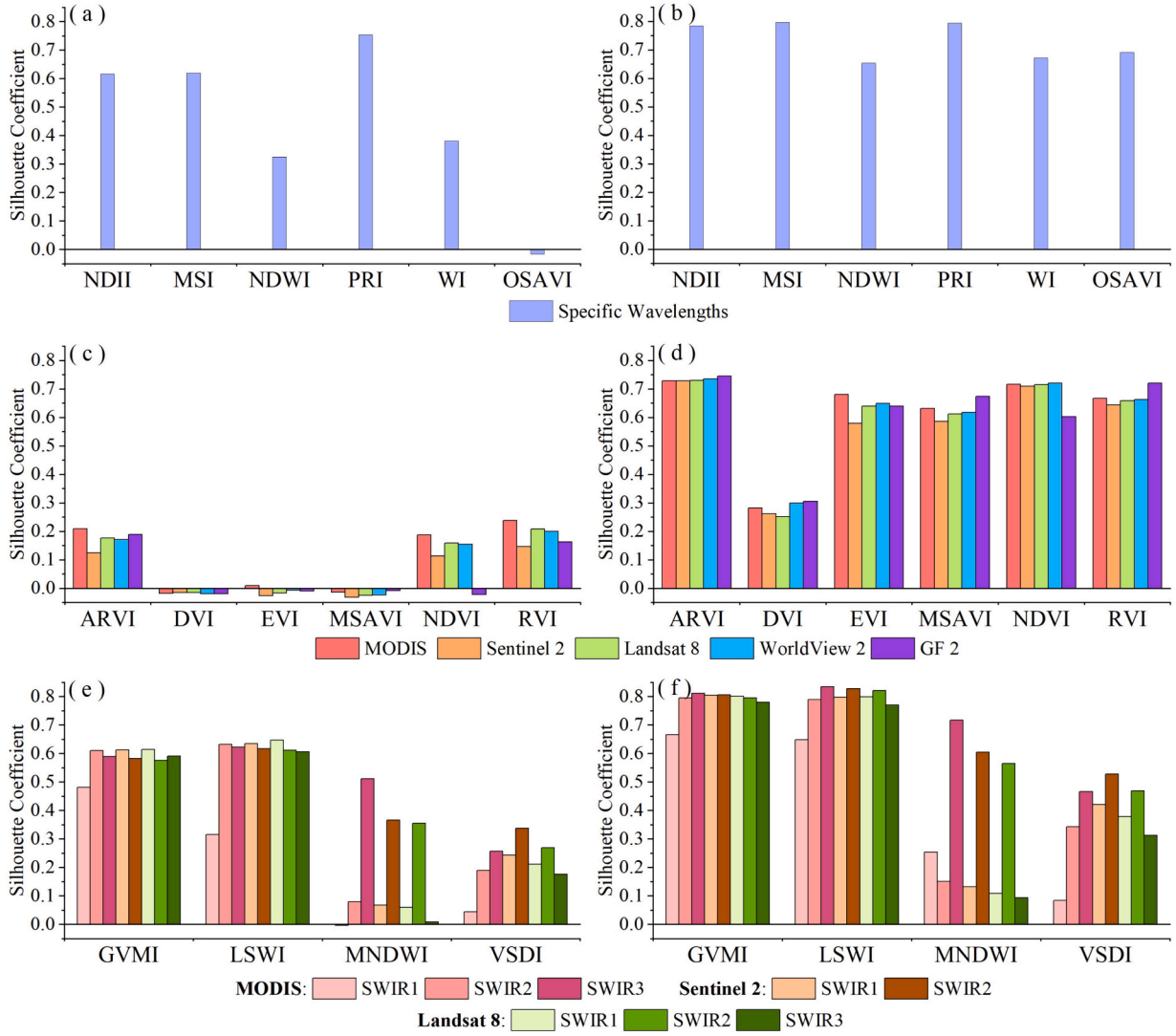

Fig. 4. Silhouette coefficient results of three type vegetation indices during growing stage (a, c and e) and stable stage (b, d and f) (Note: vegetation indices in a and b were calculated from specific wavelengths; vegetation indices in c and d were calculated from NIR and visual bands; vegetation indices in e and f were calculated from SWIR and other bands).

capabilities within the SWIR band.

Based on the calculation of 10 vegetation indices using simulated satellite band reflectance data (as shown in Fig. 4), it can be observed that among the vegetation indices calculated using the NIR region, the data obtained from MODIS have the highest silhouette coefficient. During the stable stage, the results obtained from GF2 data perform better than those from other satellites, while the results obtained from WorldView 2 data are the least favorable among the five satellites. It is worth noting that WorldView 2 and GF 2 lack reflectance data in the SWIR region, so the evaluation only included data from MODIS, Sentinel 2, and Landsat 8 in the SWIR band.

The results indicate that within the SWIR region, the best-performing band is MODIS's band 7, followed by Sentinel 2's band 12 and Landsat 8's band 7. The poorest results are associated with MODIS's band 5. Therefore, considering the overall performance across all spectral bands and the range of available satellite data, MODIS data are found to be the most suitable for grassland drought monitoring, while WorldView2 data are the least suitable.

4. Discussion

We employed the PROSAIL model to simulate grassland spectra under varying growth stages and drought conditions. Influenced by parameters predominating in different spectral bands, the response of grassland canopy reflectance to drought varies across the visible, NIR, and SWIR regions. Through ANOVA analysis, we identified four bands sensitive to moisture across diverse growth stages, which are within the ranges of 540 nm–720 nm, 1250 nm–1690 nm, 1805 nm–2190 nm, and 2264 nm–2500 nm. Notably, these sensitive bands in the visible spectrum (540–720 nm) are correlated with pigment concentration (Jiang and Carrow, 2005). Chlorophyll absorption occurs in the red and blue spectral bands, affecting the two shoulders of the green band, whereas carotenoid absorption takes place in the blue band, influencing only one side of the green band (Hong et al., 2019). When moisture decreases, vegetation closes its stomata, leading to a reduction in CO2 assimilation, a decrease in chlorophyll concentration, and a gradual decline in photosynthetic activity (Fariaszewska et al., 2020). In the NIR region, typical healthy leaves do not exhibit strong absorption characteristics, and the magnitude of reflectance is controlled by structural discontinuities encountered in the leaf (Jiang and Carrow, 2005). Under drought stress, the reflectance in the NIR region initially increases and then decreases. The increase in reflectance is attributed to the contraction of leaf mesophyll cells and the enlargement of air spaces within the leaf (Żelazny and Lukáš, 2020). Subsequently, as the leaf area decreases and

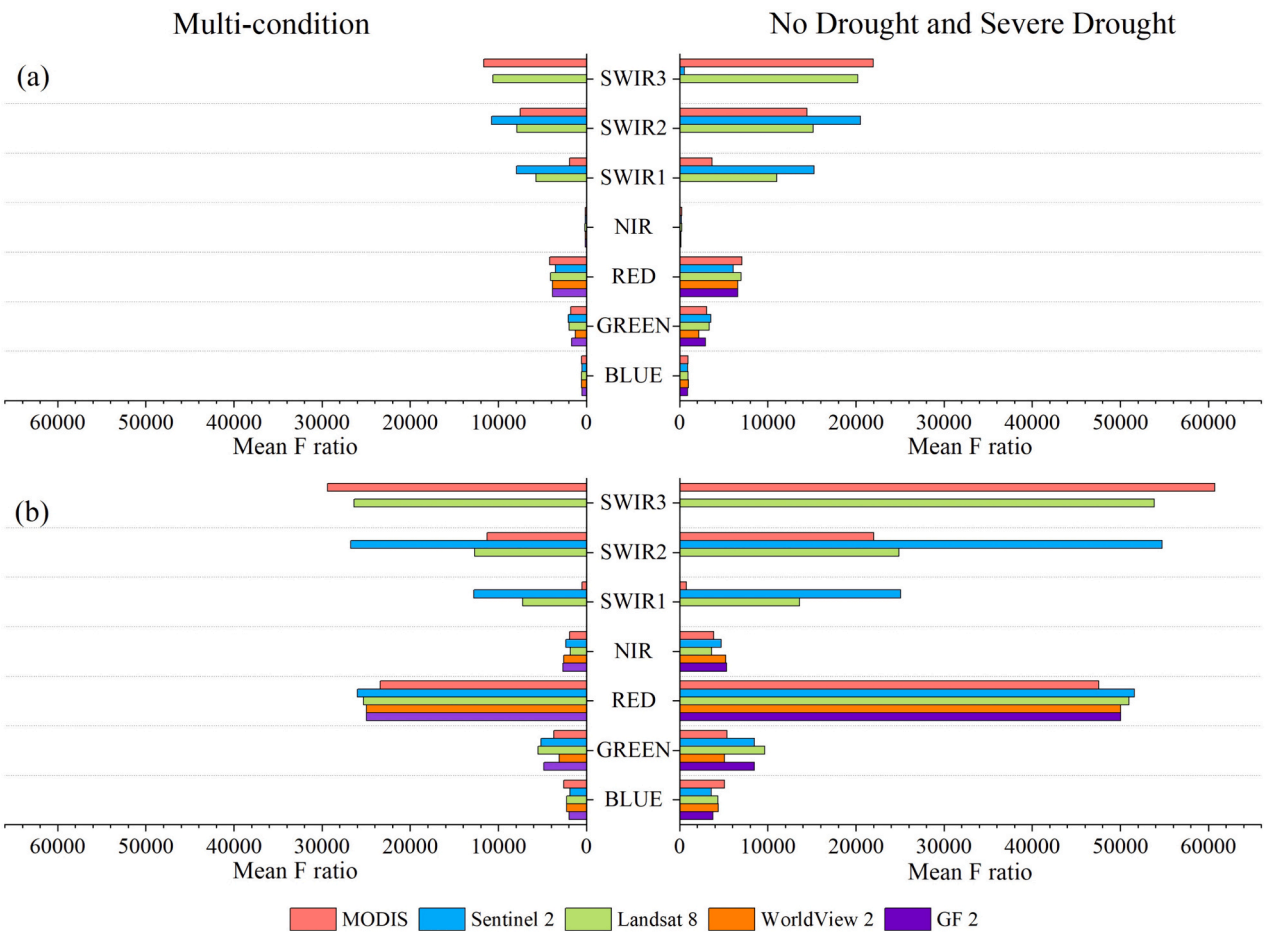

Fig. 5. Suitability of satellite bands for drought monitoring during different growth stages. Growing stage (a); Stable stage (b).

intercellular scattering in the NIR region diminishes, reflectance decreases with leaf aging. In addition, consistently with previous research, the moisture sensitive wavelengths detected during growing stage in this study are at wavelengths of 970 nm and 1200 nm, both of which are NIR bands sensitive to leaf tissue moisture content (Jiang and Carrow, 2007). For green vegetation, reflectance in the SWIR region is mainly controlled by vegetation water content (specifically, manifested as strong absorption of water), as well as the internal structure and dry matter content of the leaves (Davidson et al., 2006; Tucker, 1978). Our results show that the peaks of the F ratios are at about 1450 nm and 1930 nm in the SWIR region, which are the two main water absorption bands related to the equivalent water thickness of vegetation. Many studies have used these two wavelengths to estimate the water status of vegetation (González-Fernández et al., 2015; Rallo et al., 2014).

In this study, we assessed the grassland drought monitoring capabilities of various vegetation indices using S and SI from the perspective of vegetation water content and greenness. The results indicate that vegetation indices calculated based on the SWIR bands, with a particular emphasis on the contrast between the NIR and SWIR bands, outperformed other indices in both growth stages. Indices like DVI, EVI, and NDVI are computed based on the red and NIR bands, which are primarily affected by physiological parameters like chlorophyll content. However, changes in chlorophyll content due to drought are relatively slow compared to variations in vegetation water content (Bayat et al., 2016; Liu et al., 2004). In contrast, the reduction in water content directly leads to a decrease in reflectance. The range between 1300 nm and 2500 nm is a strong water absorption band, making it highly sensitive to variations in vegetation water content (Carter, 1991; Davidson et al., 2006; Faurtyot and Baret, 1997). Combining the NIR and SWIR regions to calculate drought index can help mitigate the influence of leaf internal structure and dry matter content, thereby enhancing the canopy moisture content information (Rallo et al., 2014). For instance, Bajgain et al. (2015) monitored drought in the high plateau grasslands of Oklahoma, USA, from 2000 to 2013. They found that the LSWI exhibited larger variations in drought and wet years when compared to the NDVI and EVI. Sow et al. (2013) calculated multiple vegetation indices using MODIS data and analyzed their correlations with measured equivalent water thickness in grasslands. They found that the NDII, MSI, and GVMI exhibited higher correlations with the EWT than the NDWI. Furthermore, considering the simulated leaf reflectance and atmospheric transmission characteristics, the shortwave infrared band in the range of 1550–1750 nm has been identified as most suitable for observing vegetation canopy moisture status (Tucker, 1980). This finding is consistent with our assessment results, indicating that bands such as MODIS band 6 (SWIR2), Sentinel-2 band 11 (SWIR1), and Landsat 8 band 6 (SWIR1), which are situated within the range of 1550–1750 nm, exhibit superior capabilities for growing stage drought monitoring compared to indices derived from other shortwave infrared bands. Therefore, vegetation indices calculated using the NIR and SWIR bands are better suited for grassland drought monitoring using multispectral satellite data. In addition, PRI calculated using hyperspectral data can capture variations in vegetation canopy moisture content under sunlight and shade, thereby demonstrating good performance in detecting early-stage vegetation water stress (Behmann et al., 2014).

Compared to previous studies, this research comprehensively evaluates the drought response of grasslands between 400 and 2500 nm as drought intensity increases. Additionally, it provides a more comprehensive assessment of the ability of vegetation indices to monitor

grassland drought by considering their sensitivity to various biochemical parameters. Previous studies often directly used satellite data for drought monitoring, with limited comparison of the drought monitoring capabilities of different satellite systems (Leisenheimer et al., 2024; Miller et al., 2022; Wang et al., 2023). This paper evaluates the suitability of commonly used satellites and satellite bands for grassland drought monitoring through extensive coverage of simulated reflectance curves and spectral response functions across various conditions. The results provide valuable guidance for researchers and practitioners when selecting data and monitoring indicators. Additionally, the study's findings can serve as a theoretical foundation for designing new sensors and remote sensing drought indices based on existing sensitive bands and drought indices. Furthermore, the analysis was conducted separately for different growth stages of grassland, considering potential variations in vegetation structure and spectral characteristics, thereby enhancing the applicability of the research results throughout the growth cycle.

However, this study still has certain limitations. First, the simulated grassland spectra in this research have some constraints. Due to condition limitations, it was not possible to simulate finer growth stages. In addition, the types of grassland vary in different regions due to environmental factors, and different grass species exhibit varying degrees of sensitivity to drought (Lin et al., 2021): C_3 grasses respond to drought by closing their stomata to minimize water loss, while C_4 grasses do not adjust stomatal conductance in the early stages of drought. However, both types of grasses suppress photosynthetic rates under drought conditions (Lemoine et al., 2018). Therefore, further refinement of the results is needed with more diverse grassland types and growth stages to enhance the universality of the findings. When assessing the drought monitoring capabilities of satellites, the analysis in this study primarily focused on the spectral perspective, examining the match between sensitive bands and different vegetation index calculations. However, aspects such as satellite revisit frequency, spatial resolution, and practical suitability for grassland drought monitoring were not thoroughly analyzed. Future research should integrate these considerations into the assessment after practical application.

5. Conclusion

This study used the PROSAIL model to simulate canopy spectral curves of grasslands across various growth stages and drought conditions. It conducted a comparative analysis of the suitability of five commonly used satellites (MODIS, Sentinel 2, Landsat 8, WorldView 2, GF 2) and 16 frequently employed vegetation indices (NDVI, EVI, RVI, DVI, MSAVI, ARVI, MNDWI, GVMI, LSWI, VSDI, WI, MSI, NDWI, NDII, PRI, and OSAVI) for monitoring grassland drought. The analysis revealed that: (1) Within the spectral range of 400 nm to 2500 nm, both growth stages of grasslands exhibited sensitivity in four wavelength intervals related to moisture content, primarily concentrated in the red and shortwave infrared spectral bands. These intervals were identified as 540 nm–720 nm, 1250 nm–1690 nm, 1805 nm–2190 nm, and 2264 nm–2500 nm. (2) Indices calculated using the infrared-shortwave infrared spectral range were found to be more suitable for grassland drought monitoring than those computed using the red and near-infrared spectral range. Among the 16 vegetation indices analyzed, PRI was the most suitable index for grassland drought monitoring during the growing stage, while LSWI and GVMI were most suitable during the stable stage. NDII, MSI, PRI, LSWI, and GVMI were suitable for both growth stages, while DVI was found to be unsuitable for monitoring grassland drought. (3) In terms of the sensitivity to changes in moisture content and the suitability of satellite-derived indices for drought monitoring, MODIS is the most suitable satellite. Within the satellite bands, MODIS band 7 was identified as the most sensitive to moisture changes.

Funding

This work was supported by the National Key Research and Development Program of China (Grant No. 2021YFB3901201); the National Natural Science Foundation of China (Grant No. 42077436); and the Open Fund of State Key Laboratory of Remote Sensing Science and Beijing Engineering Research Center for Global Land Remote Sensing Products (Grant No. OF202215).

CRediT authorship contribution statement

Xiufang Zhu: Writing – review & editing, Methodology, Funding acquisition, Conceptualization. **Qingfen Li:** Writing – original draft, Methodology, Investigation, Formal analysis, Conceptualization. **Chunhua Guo:** Writing – original draft, Methodology, Investigation.

Declaration of competing interest

The authors declare that they have no known competing financial interests or personal relationships that could have appeared to influence the work reported in this paper.

Data availability

Data will be made available on request.

Appendix A. Separation index results

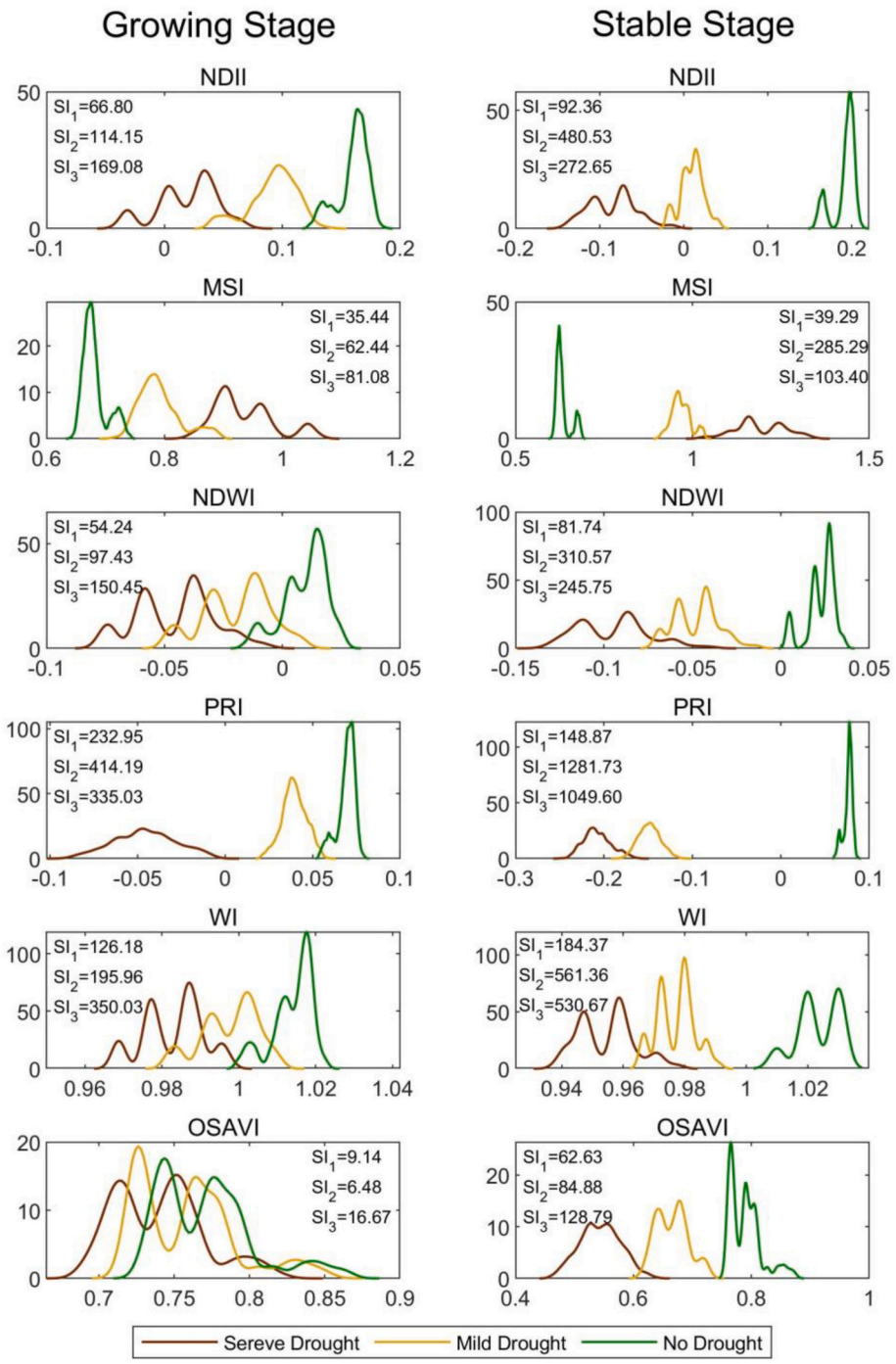

Fig. A1. Separability degree between the index values of hyperspectral vegetation indices under no drought, mild drought and severe drought condition in both growth stages. (Note: SI_1 represents the separation index between severe and mild drought condition; SI_2 represents the separation index between mild and no drought condition; SI_3 represents the separation index between severe and no drought condition.)

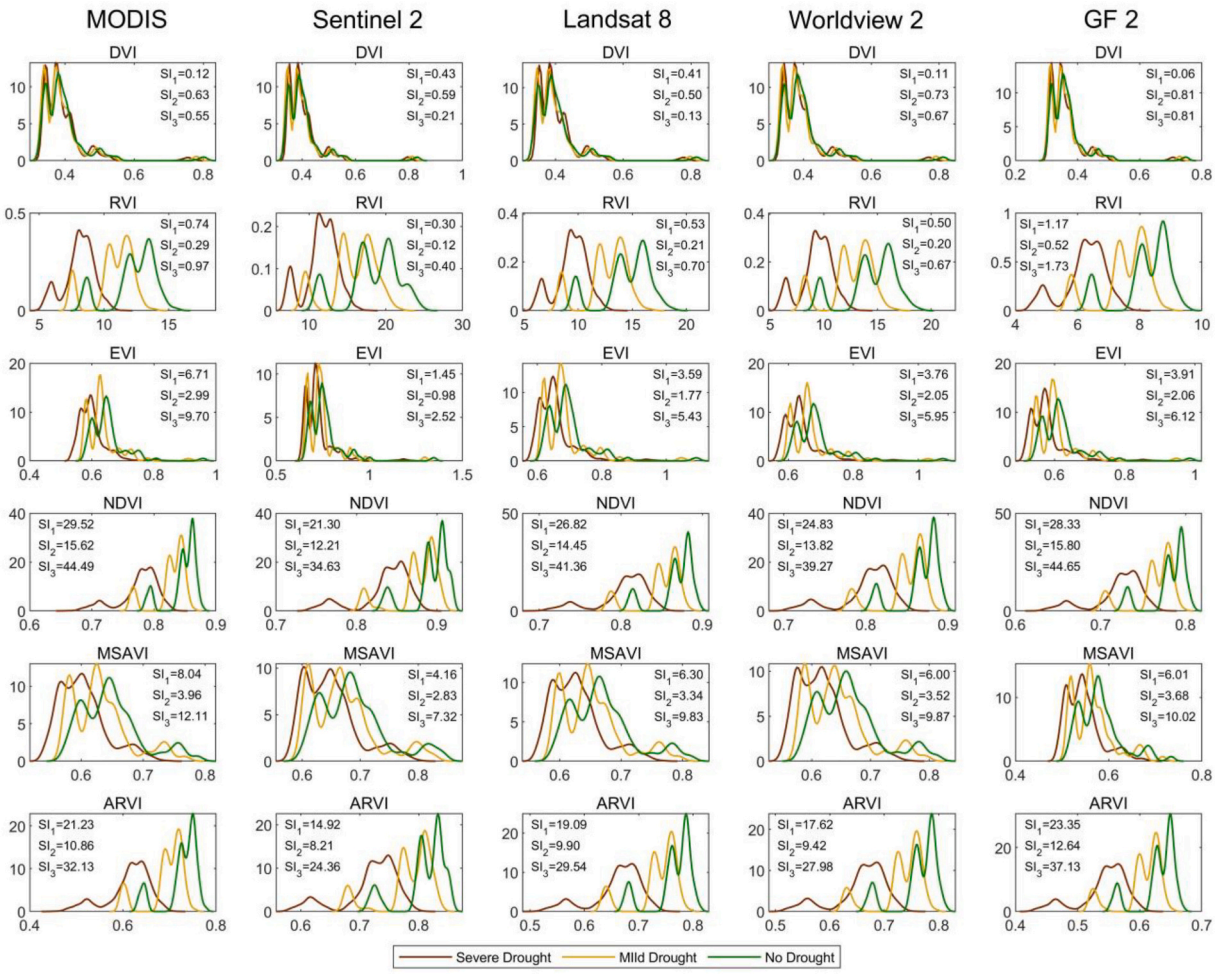

Fig. A2. Separability degree between the index values of vegetation indices that was calculated by NIR band and other visible bands under no drought, mild drought and severe drought condition in growing stage. The meaning of SI_1, SI_2, SI_3 is the same as Fig. 1.

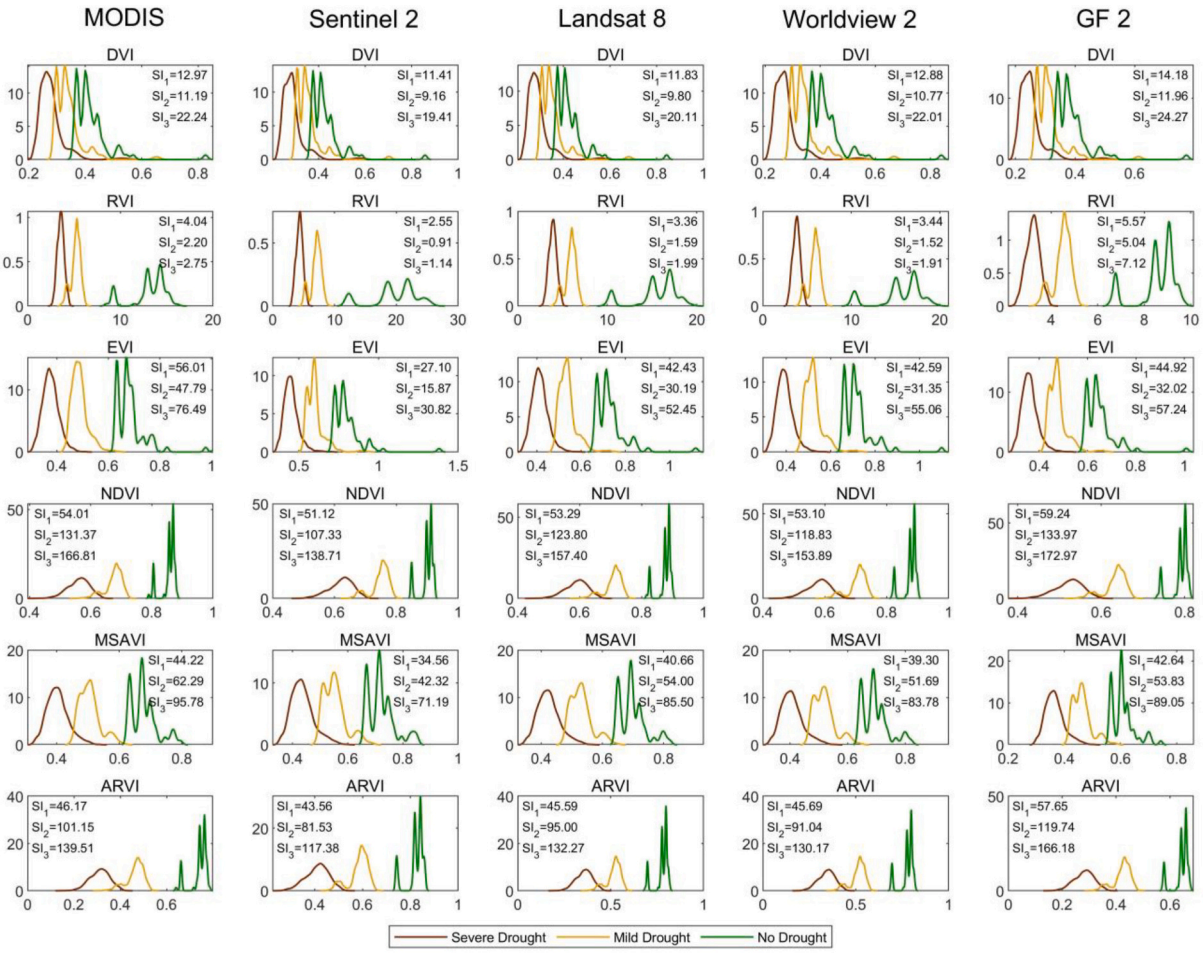

Fig. A3. Separability degree between the index values of vegetation indices that was calculated by NIR band and other visible bands under no drought, mild drought and severe drought condition in stable stage. The meaning of SI_1, SI_2, SI_3 is the same as Fig. 1.

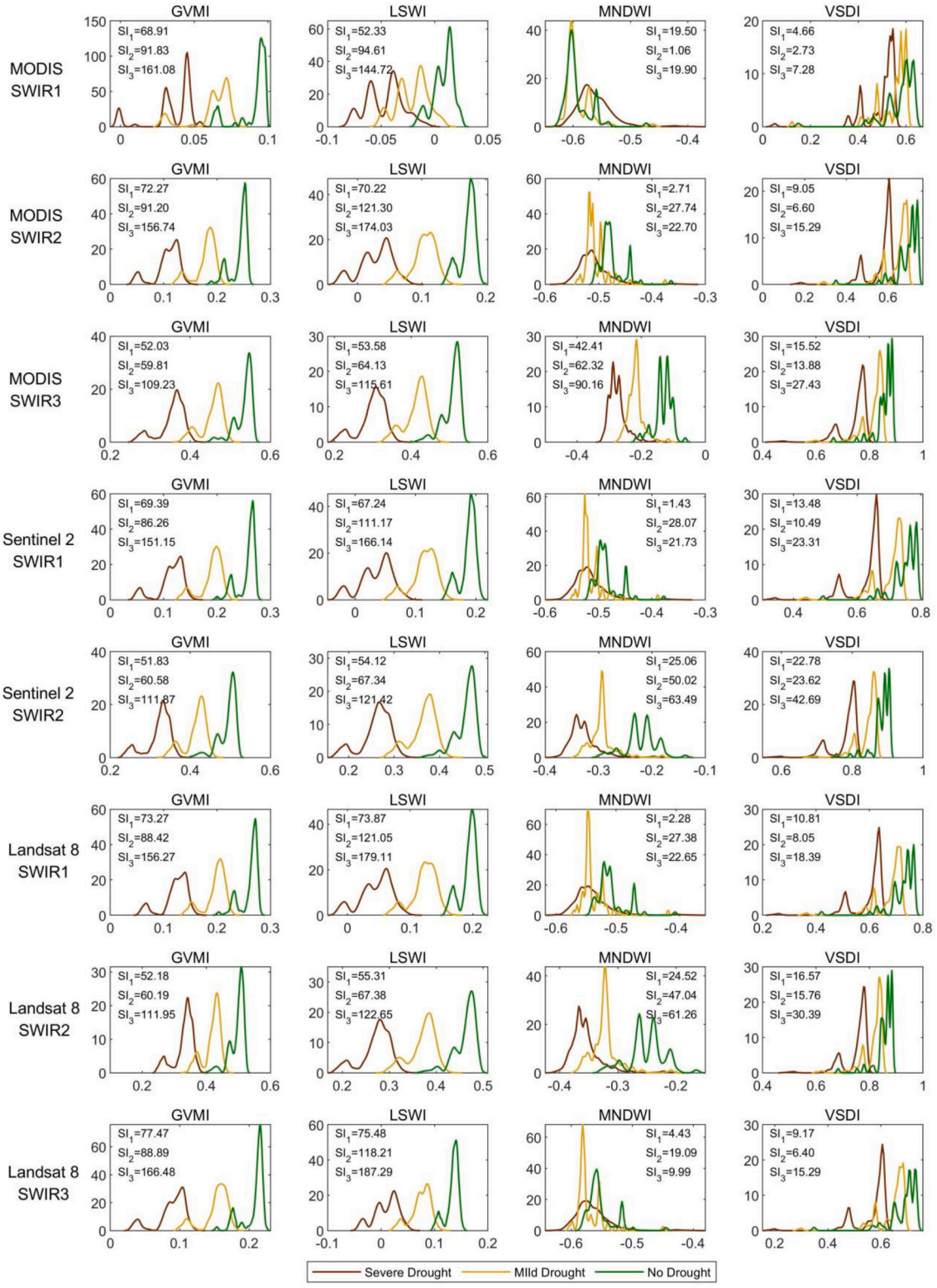

Fig. A4. Separability degree between the index values of vegetation indices that was calculated by SWIR band and other bands under no drought, mild drought and severe drought condition in growing stage. The meaning of SI_1, SI_2, SI_3 is the same as Fig. 1.

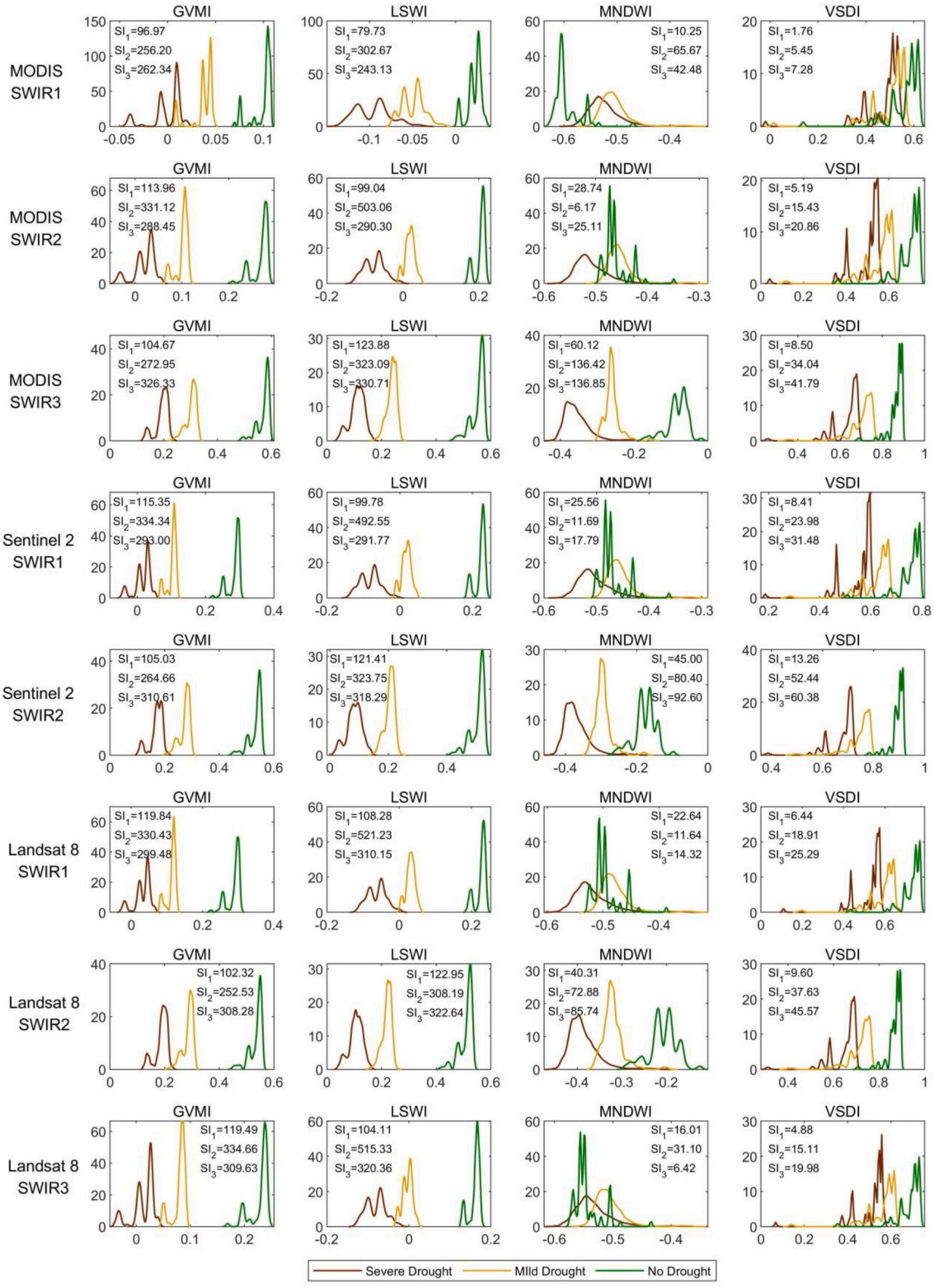

Fig. A5. Separability degree between the index values of vegetation indices that was calculated by SWIR band and other bands under no drought, mild drought and severe drought condition in stable stage. The meaning of SI_1, SI_2, SI_3 is the same as Fig. 1.

References

Alahacoon, N., Edirisinghe, M., 2022. A comprehensive assessment of remote sensing and traditional based drought monitoring indices at global and regional scale. Geomat. Nat. Haz. Risk 13 (1), 762–799.

Almeida-Ñauñay, A.F., Villeta, M., Quemada, M., Tarquis, A.M., 2022. Assessment of drought indexes on different time scales: a case in semiarid mediterranean grasslands. Remote Sens. 14 (3), 565.

Ashraf, M., Ullah, K., Adnan, S., 2022. Satellite based impact assessment of temperature and rainfall variability on drought indices in southern Pakistan. Int. J. Appl. Earth Obs. Geoinf. 108, 102726.

Atzberger, C., Darvishzadeh, R., Schlerf, M., Le Maire, G., 2013. Suitability and adaptation of PROSAIL radiative transfer model for hyperspectral grassland studies. Remote Sens. Lett. 4 (1), 55–64.
Bagirov, A.M., Aliguliyev, R.M., Sultanova, N., 2023. Finding compact and well-separated clusters: clustering using silhouette coefficients. Pattern Recogn. 135, 109144.
Bajgain, R., Xiao, X., Wagle, P., Basara, J., Zhou, Y., 2015. Sensitivity analysis of vegetation indices to drought over two tallgrass prairie sites. ISPRS J. Photogramm. Remote Sens. 108, 151–160.
Bayat, B., Van der Tol, C., Verhoef, W., 2016. Remote sensing of grass response to drought stress using spectroscopic techniques and canopy reflectance model inversion. Remote Sens. 8 (7), 557.
Behifar, M., Kakroodi, A., Kiavarz, M., Azizi, G., 2023. Satellite-based drought monitoring using optimal indices for diverse climates and land types. Eco. Inform. 76, 102143.
Behmann, J., Steinrücken, J., Plümer, L., 2014. Detection of early plant stress responses in hyperspectral images. ISPRS J. Photogramm. Remote Sens. 93, 98–111.
Berger, K., Atzberger, C., Danner, M., D'Urso, G., Mauser, W., Vuolo, F., Hank, T., 2018. Evaluation of the PROSAIL model capabilities for future hyperspectral model environments: a review study. Remote Sens. 10 (1), 85.
Cârlan, I., Mihai, B.-A., Nistor, C., Große-Stoltenberg, A., 2020. Identifying urban vegetation stress factors based on open access remote sensing imagery and field observations. Eco. Inform. 55, 101032.
Carter, G.A., 1991. Primary and secondary effects of water content on the spectral reflectance of leaves. Am. J. Bot. 78 (7), 916–924.
Ceccato, P., Gobron, N., Flasse, S., Pinty, B., Tarantola, S., 2002. Designing a spectral index to estimate vegetation water content from remote sensing data: part 1: theoretical approach. Remote Sens. Environ. 82 (2–3), 188–197.
Chang, S., Wu, B., Yan, N., Davdai, B., Nasanbat, E., 2017. Suitability assessment of satellite-derived drought indices for Mongolian grassland. Remote Sens. 9 (7), 650.
Chang, S., Chen, H., Wu, B., Nasanbat, E., Yan, N., Davdai, B., 2021. A practical satellite-derived vegetation drought index for arid and semi-arid grassland drought monitoring. Remote Sens. 13 (3), 414.
Colombo, R., Meroni, M., Marchesi, A., Busetto, L., Rossini, M., Giardino, C., Panigada, C., 2008. Estimation of leaf and canopy water content in poplar plantations by means of hyperspectral indices and inverse modeling. Remote Sens. Environ. 112 (4), 1820–1834.
Davidson, A., Wang, S., Wilmshurst, J., 2006. Remote sensing of grassland–shrubland vegetation water content in the shortwave domain. Int. J. Appl. Earth Obs. Geoinf. 8 (4), 225–236.
Demetriades-Shah, T.H., Steven, M.D., Clark, J.A., 1990. High resolution derivative spectra in remote sensing. Remote Sens. Environ. 33 (1), 55–64.
Ding, Y., Xu, J., Wang, X., Peng, X., Cai, H., 2020. Spatial and temporal effects of drought on Chinese vegetation under different coverage levels. Sci. Total Environ. 716, 137166.
Duarte, L., Teodoro, A., Gonçalves, H., 2014. Deriving phenological metrics from NDVI through an open source tool developed in QGIS. In: Earth Resources and Environmental Remote Sensing/GIS Applications V.
English, S., Lean, P., Geer, A., 2020. How radiative transfer models can support the future needs of earth-system forecasting and re-analysis. J. Quant. Spectrosc. Radiat. Transf. 251, 107044.
Fariaszewska, A., Aper, J., Van Huylenbroeck, J., De Swaef, T., Baert, J., Pecio, Ł., 2020. Physiological and biochemical responses of forage grass varieties to mild drought stress under field conditions. Int. J. Plant Prod. 14 (2), 335–353.
Faurtyot, T., Baret, F., 1997. Vegetation water and dry matter contents estimated from top-of-the-atmosphere reflectance data: a simulation study. Remote Sens. Environ. 61 (1), 34–45.
Féret, J.-B., Gitelson, A., Noble, S., Jacquemoud, S., 2017. PROSPECT-D: towards modeling leaf optical properties through a complete lifecycle. Remote Sens. Environ. 193, 204–215.
Gamon, J., Penuelas, J., Field, C., 1992. A narrow-waveband spectral index that tracks diurnal changes in photosynthetic efficiency. Remote Sens. Environ. 41 (1), 35–44.
Gao, B.-C., 1996. NDWI—A normalized difference water index for remote sensing of vegetation liquid water from space. Remote Sens. Environ. 58 (3), 257–266.
Gessner, U., Reinermann, S., Asam, S., Kuenzer, C., 2023. Vegetation stress monitor—assessment of drought and temperature-related effects on vegetation in Germany analyzing MODIS time series over 23 years. Remote Sens. 15 (22), 5428.
Ghasempour, R., Aalami, M.T., Saghebian, S.M., Kirca, V.O., 2024. Analysis of spatiotemporal variations of drought and soil salinity via integrated multiscale and remote sensing-based techniques (case study: Urmia Lake basin). Eco. Inform. 81, 102560.
González-Fernández, A.B., Rodríguez-Pérez, J.R., Marcelo, V., Valenciano, J.B., 2015. Using field spectrometry and a plant probe accessory to determine leaf water content in commercial vineyards. Agric. Water Manag. 156, 43–50.
Henchiri, M., Liu, Q., Essifi, B., Javed, T., Zhang, S., Bai, Y., Zhang, J., 2020. Spatio-temporal patterns of drought and impact on vegetation in north and West Africa based on multi-satellite data. Remote Sens. 12 (23), 3869.
Hong, M., Bremer, D.J., van Der Merwe, D., 2019. Using small unmanned aircraft systems for early detection of drought stress in turfgrass. Crop Sci. 59 (6), 2829–2844.
Huete, A., Didan, K., Miura, T., Rodriguez, E.P., Gao, X., Ferreira, L.G., 2002. Overview of the radiometric and biophysical performance of the MODIS vegetation indices. Remote Sens. Environ. 83 (1–2), 195–213.
Hunt Jr., E.R., Rock, B.N., Nobel, P.S., 1987. Measurement of leaf relative water content by infrared reflectance. Remote Sens. Environ. 22 (3), 429–435.
Jackson, T.J., Chen, D., Cosh, M., Li, F., Anderson, M., Walthall, C., Doriaswamy, P., Hunt, E.R., 2004. Vegetation water content mapping using Landsat data derived normalized difference water index for corn and soybeans. Remote Sens. Environ. 92 (4), 475–482.
Jacquemoud, S., Baret, F., 1990. PROSPECT: a model of leaf optical properties spectra. Remote Sens. Environ. 34 (2), 75–91.
Jiang, Y., Carrow, R.N., 2005. Assessment of narrow-band canopy spectral reflectance and turfgrass performance under drought stress. HortScience 40 (1), 242–245.
Jiang, Y., Carrow, R.N., 2007. Broadband spectral reflectance models of turfgrass species and cultivars to drought stress. Crop Sci. 47 (4), 1611–1618.
Jin, J., Wang, Q., 2016. Hyperspectral indices based on first derivative spectra closely trace canopy transpiration in a desert plant. Eco. Inform. 35, 1–8.
Jordan, C.F., 1969. Derivation of leaf-area index from quality of light on the forest floor. Ecology 50 (4), 663–666.
Jupp, D.L., Strahler, A.H., 1991. A hotspot model for leaf canopies. Remote Sens. Environ. 38 (3), 193–210.
Kaufman, Y.J., Remer, L.A., 1994. Detection of forests using mid-IR reflectance: an application for aerosol studies. IEEE Trans. Geosci. Remote Sens. 32 (3), 672–683.
Kaufman, Y.J., Tanre, D., 1992. Atmospherically resistant vegetation index (ARVI) for EOS-MODIS. IEEE Trans. Geosci. Remote Sens. 30 (2), 261–270.
Kogan, F.N., 1990. Remote sensing of weather impacts on vegetation in non-homogeneous areas. Int. J. Remote Sens. 11 (8), 1405–1419.
Kowalski, K., Okujeni, A., Brell, M., Hostert, P., 2022. Quantifying drought effects in central European grasslands through regression-based unmixing of intra-annual Sentinel-2 time series. Remote Sens. Environ. 268, 112781.
Leisenheimer, L., Wellmann, T., Jänicke, C., Haase, D., 2024. Monitoring drought impacts on street trees using remote sensing - disentangling temporal and species-specific response patterns with Sentinel-2 imagery. Eco. Inform. 82, 102659 https://doi.org/10.1016/j.ecoinf.2024.102659.
Lemoine, N.P., Griffin-Nolan, R.J., Lock, A.D., Knapp, A.K., 2018. Drought timing, not previous drought exposure, determines sensitivity of two shortgrass species to water stress. Oecologia 188, 965–975.
Li, M., Chu, R., Sha, X., Ni, F., Xie, P., Shen, S., Islam, A.R.M.T., 2021a. Hyperspectral characteristics and scale effects of leaf and canopy of summer maize under continuous water stresses. Agriculture 11 (12), 1180.
Li, W., Duan, L., Wang, W., Wu, Y., Liu, T., Quan, Q., Chen, X., Yin, H., Zhou, Q., 2021b. Spatiotemporal characteristics of drought in a semi-arid grassland over the past 56 years based on the standardized precipitation index. Meteorog. Atmos. Phys. 133, 41–54.
Li, Z.-L., Leng, P., Zhou, C., Chen, K.-S., Zhou, F.-C., Shang, G.-F., 2021c. Soil moisture retrieval from remote sensing measurements: current knowledge and directions for the future. Earth Sci. Rev. 218, 103673.
Li, P., Liu, Z., Zhou, X., Xie, B., Li, Z., Luo, Y., Zhu, Q., Peng, C., 2021d. Combined control of multiple extreme climate stressors on autumn vegetation phenology on the Tibetan plateau under past and future climate change. Agric. For. Meteorol. 308, 108571.
Li, Q., Gao, M., Li, Z.-L., 2022. Ground hyper-spectral remote-sensing monitoring of wheat water stress during different growing stages. Agronomy 12 (10), 2267.
Li, Z.L., Wu, H., Duan, S.B., Zhao, W., Ren, H., Liu, X., Leng, P., Tang, R., Ye, X., Zhu, J., 2023. Satellite remote sensing of global land surface temperature: definition, methods, products, and applications. Rev. Geophys. 61 (1).
Lijuan, G., Xiaoping, W., Qingtao, W., Hong, D., Chuanyan, Z., 2017. Applicability of PROSAIL model to spring wheat in semi-arid region of the loess plateau under different drought stress. J. Arid Meteorol. 35 (6), 926.
Lin, S., Li, J., Liu, Q., Gioli, B., Paul-Limoges, E., Buchmann, N., Gharun, M., Hörtnagl, L., Foltýnová, L., Dušek, J., 2021. Improved global estimations of gross primary productivity of natural vegetation types by incorporating plant functional type. Int. J. Appl. Earth Obs. Geoinf. 100, 102328.
Liu, L., Wang, J., Huang, W., Zhao, C., Zhang, B., Tong, Q., 2004. Estimating winter wheat plant water content using red edge parameters. Int. J. Remote Sens. 25 (17), 3331–3342.
Liu, Q., Zhang, S., Zhang, H., Bai, Y., Zhang, J., 2020. Monitoring drought using composite drought indices based on remote sensing. Sci. Total Environ. 711, 134585.
Liu, X., Zhu, Z., Liu, X., Yu, M., 2021. Thresholds of key disaster-inducing factors and drought simulation in the Xilinguole grassland. Eco. Inform. 64, 101380.
Liu, X., Liu, X., Yu, M., Zhu, Z., 2022. Characteristics and driving conditions of flash drought in different grassland ecosystems. Sci. Total Environ. 849, 157923 https://doi.org/10.1016/j.scitotenv.2022.157923.
Miller, D.L., Alonzo, M., Meerdink, S.K., Allen, M.A., Tague, C.L., Roberts, D.A., McFadden, J.P., 2022. Seasonal and interannual drought responses of vegetation in a California urbanized area measured using complementary remote sensing indices. ISPRS J. Photogramm. Remote Sens. 183, 178–195.
Mpelasoka, F., Hennessy, K., Jones, R., Bates, B., 2008. Comparison of suitable drought indices for climate change impacts assessment over Australia towards resource management. Int. J. Climatol. 28 (10), 1283–1292.
Peng, J., Dong, W., Yuan, W., Zhang, Y., 2012. Responses of grassland and forest to temperature and precipitation changes in Northeast China. Adv. Atmos. Sci. 29, 1063–1077.
Peñuelas, J., Pinol, J., Ogaya, R., Filella, I., 1997. Estimation of plant water concentration by the reflectance water index WI (R900/R970). Int. J. Remote Sens. 18 (13), 2869–2875.
Perry, E.M., Roberts, D.A., 2008. Sensitivity of narrow-band and broad-band indices for assessing nitrogen availability and water stress in an annual crop. Agron. J. 100 (4), 1211–1219.
Qi, J., Chehbouni, A., Huete, A.R., Kerr, Y.H., Sorooshian, S., 1994. A modified soil adjusted vegetation index. Remote Sens. Environ. 48 (2), 119–126.

Qin, Q., Wu, Z., Zhang, T., Sagan, V., Zhang, Z., Zhang, Y., Zhang, C., Ren, H., Sun, Y., Xu, W., 2021. Optical and thermal remote sensing for monitoring agricultural drought. Remote Sens. 13 (24), 5092.
Rallo, G., Minacapilli, M., Ciraolo, G., Provenzano, G., 2014. Detecting crop water status in mature olive groves using vegetation spectral measurements. Biosyst. Eng. 128, 52–68.
Ranjan, R., Sahoo, R., Chopra, U., Pramanik, M., Singh, A., Pradhan, S., 2017. Assessment of water status in wheat (*Triticum aestivum* L.) using ground based hyperspectral reflectance. In: Proceedings of the National Academy of Sciences, India Section B: Biological Sciences, 87, pp. 377–388.
Rondeaux, G., Steven, M., Baret, F., 1996. Optimization of soil-adjusted vegetation indices. Remote Sens. Environ. 55 (2), 95–107.
Sall, I., Jarchow, C.J., Sigafus, B.H., Eby, L.A., Forzley, M.J., Hossack, B.R., 2021. Estimating inundation of small waterbodies with sub-pixel analysis of Landsat imagery: long-term trends in surface water area and evaluation of common drought indices. Remote Sens. Ecol. Conserv. 7 (1), 109–124.
Sow, M., Mbow, C., Hély, C., Fensholt, R., Sambou, B., 2013. Estimation of herbaceous fuel moisture content using vegetation indices and land surface temperature from MODIS data. Remote Sens. 5 (6), 2617–2638.
Szabo, S., Gácsi, Z., Balazs, B., 2016. Specific features of NDVI, NDWI and MNDWI as reflected in land cover categories. Acta geographica Debrecina. Landscape Environ. Ser. 10 (3/4), 194.
Tucker, C.J., 1978. A comparison of satellite sensor bands for vegetation monitoring. Photogramm. Eng. Remote. Sens. 44 (11), 1369–1380.
Tucker, C.J., 1979. Red and photographic infrared linear combinations for monitoring vegetation. Remote Sens. Environ. 8 (2), 127–150.
Tucker, C.J., 1980. Remote sensing of leaf water content in the near infrared. Remote Sens. Environ. 10 (1), 23–32.
Varghese, D., Radulović, M., Stojković, S., Crnojević, V., 2021. Reviewing the potential of Sentinel-2 in assessing the drought. Remote Sens. 13 (17), 3355.
Verhoef, W., 1984. Light scattering by leaf layers with application to canopy reflectance modeling: the SAIL model. Remote Sens. Environ. 16 (2), 125–141.
Wang, X., Zhao, C., Guo, N., Li, Y., Jian, S., Yu, K., 2015. Determining the canopy water stress for spring wheat using canopy hyperspectral reflectance data in loess plateau semiarid regions. Spectrosc. Lett. 48 (7), 492–498.
Wang, X.-D., Xu, H.-J., Pan, Y.-X., Fu, G.-Q., Chen, T., Qi, X.-L., Yang, X.-M., 2023. Vegetation responses to ecological water delivery and prolonged droughts in an artificial desert oasis, Northwestern China. Ecol. Inform. 77, 102284 https://doi.org/10.1016/j.ecoinf.2023.102284.
Wei, W., Zhang, J., Zhou, L., Xie, B., Zhou, J., Li, C., 2021. Comparative evaluation of drought indices for monitoring drought based on remote sensing data. Environ. Sci. Pollut. Res. 28, 20408–20425.
West, H., Quinn, N., Horswell, M., 2019. Remote sensing for drought monitoring & impact assessment: Progress, past challenges and future opportunities. Remote Sens. Environ. 232, 111291.
Xiang, K., Yuan, W., Wang, L., Deng, Y., 2020. An LSWI-based method for mapping irrigated areas in China using moderate-resolution satellite data. Remote Sens. 12 (24), 4181.
Xing, N., Huang, W., Ye, H., Ren, Y., Xie, Q., 2021. Joint retrieval of winter wheat leaf area index and canopy chlorophyll density using hyperspectral vegetation indices. Remote Sens. 13 (16), 3175.
Yu, X., Guo, X., 2023. Inter-annual drought monitoring in northern mixed grasslands by a revised vegetation health index from historical Landsat imagery. J. Arid Environ. 213, 104964.
Želazny, W.R., Lukáš, J., 2020. Drought stress detection in juvenile oilseed rape using hyperspectral imaging with a focus on spectra variability. Remote Sens. 12 (20), 3462.
Zhang, F., Zhou, G., 2015. Estimation of canopy water content by means of hyperspectral indices based on drought stress gradient experiments of maize in the north plain China. Remote Sens. 7 (11), 15203–15223.
Zhang, N., Hong, Y., Qin, Q., Liu, L., 2013. VSDI: a visible and shortwave infrared drought index for monitoring soil and vegetation moisture based on optical remote sensing. Int. J. Remote Sens. 34 (13), 4585–4609.
Zhang, C., Pattey, E., Liu, J., Cai, H., Shang, J., Dong, T., 2017. Retrieving leaf and canopy water content of winter wheat using vegetation water indices. IEEE J. Select. Top. Appl. Earth Observ. Remote Sens. 11 (1), 112–126.
Zhang, R., Liang, T., Guo, J., Xie, H., Feng, Q., Aimaiti, Y., 2018. Grassland dynamics in response to climate change and human activities in Xinjiang from 2000 to 2014. Sci. Rep. 8 (1), 2888.
Zhao, Q., Yu, L., Du, Z., Peng, D., Hao, P., Zhang, Y., Gong, P., 2022. An overview of the applications of earth observation satellite data: impacts and future trends. Remote Sens. 14 (8), 1863.
Zhao, A., Xu, R., Zou, L., Zhu, X., 2023. Response of grassland vegetation growth to drought in Inner Mongolia of China from 2002 to 2020. Atmosphere 14 (11), 1613.
Zhou, J.-J., Zhang, Y.-H., Han, Z.-M., Liu, X.-Y., Jian, Y.-F., Hu, C.-G., Dian, Y.-Y., 2021. Evaluating the performance of hyperspectral leaf reflectance to detect water stress and estimation of photosynthetic capacities. Remote Sens. 13 (11), 2160.